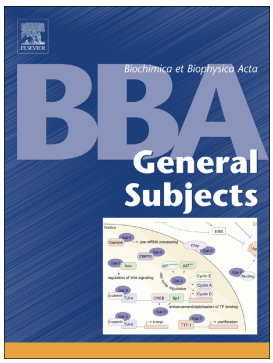

Covalent inhibition of histone deacetylase 8 by 3,4-dihydro-2H-pyrimido[1,2-c][1,3]benzothiazin-6-imine

Marius Muth, Niklas Jänsch, Aleksandra Kopranovic, Andreas Krämer, Nathalie Wössner, Manfred Jung, Frank Kirschhöfer, Gerald Brenner-Weiß, Franz-Josef Meyer-Almes

PII: S0304-4165(19)30001-7
DOI: https://doi.org/10.1016/j.bbagen.2019.01.001
Reference: BBAGEN 29279

To appear in: *BBA - General Subjects*

Received date: 31 August 2018
Revised date: 25 November 2018
Accepted date: 2 January 2019

Please cite this article as: Marius Muth, Niklas Jänsch, Aleksandra Kopranovic, Andreas Krämer, Nathalie Wössner, Manfred Jung, Frank Kirschhöfer, Gerald Brenner-Weiß, Franz-Josef Meyer-Almes , Covalent inhibition of histone deacetylase 8 by 3,4-dihydro-2H-pyrimido[1,2-c][1,3]benzothiazin-6-imine. Bbagen (2019), https://doi.org/10.1016/j.bbagen.2019.01.001

Covalent inhibition of histone deacetylase 8 by 3,4-dihydro-2H-pyrimido[1,2-c][1,3]benzothiazin-6-imine

Marius Muth[1,3], Niklas Jänsch[1], Aleksandra Kopranovic[1], Andreas Krämer[2], Nathalie Wössner[4], Manfred Jung[4], Frank Kirschhöfer[3], Gerald Brenner-Weiß[3], Franz-Josef Meyer-Almes[1,*]

[1] Department of Chemical Engineering and Biotechnology, University of Applied Sciences Darmstadt, Germany.

[2] Institute of Pharmaceutical Chemistry, University Frankfurt, Germany.

[3] Bioengineering and Biosystems, Institute of Functional Interfaces, Karlsruhe Institute of Technology, Germany.

[4] Institute of Pharmaceutical Sciences, University of Freiburg, Germany.

* Corresponding author:

Franz-Josef Meyer-Almes

Email : franz-josef.meyer-almes@h-da.de

Phone: +49 6151168406

Fax : +49 6151168404

Background:

HDAC8 is an established target for T-cell lymphoma and childhood neuroblastoma. Benzothiazine-imines are promising HDAC8 inhibitors with unknown binding mechanism lacking a usual zinc binding group.

Methods:

In this study high-resolution and quantitative HPLC-coupled ESI-MS / MS techniques are combined with crystal structure determination and a variety of biochemical and computational methods to elucidate the reaction mechanism between benzothiazine-imine **1** and HDAC8.

Results:

1) **1** is a covalent inhibitor of HDAC8; 2) inhibition is reversible in the presence of reducing agents; 3) C153 in the active site and C102 are involved in the inhibition mechanism; 4) **1** modifies various cysteines in HDAC8 forming either thiocyanates or mixed disulfides with **3**; 5) **1** and **5** dock in close proximity to C153 within the active site. This is supposed to accelerate covalent inactivation particularly in HDAC8 and suggested as major determinant for the observed nanomolar potency and selectivity of **1**.

Conclusions:

1 and its analogs are interesting model compounds but unsuitable for therapeutic treatment due to their high unselective reactivity towards thiol groups. However, the postulated preceding non-covalent binding mode of **1** opens a door to optimized next generation compounds that combine potent and selective non-covalent recognition with low reactivity towards C153 at the active site of HDAC8.

General Significance:

1 represents a completely new class of inhibitors for HDAC8. Initial non-covalent interaction at the bottom of the active site is suggested to be the key for its selectivity. Further optimization of non-covalent interaction and thiol-reactivity provides opportunities to develop therapeutic useful covalent HDAC8 inhibitors.

Keywords:

HDAC8, selective inhibition, binding mechanism, non-hydroxamate inhibitor, covalent inhibitor, enzyme inhibition

1. Introduction

3,4-Dihydro-2H-pyrimido[1,2-c][1,3]benzothiazin-6-imine (PD 404,182, **1**) is a known inhibitor of bacterial 3-deoxy-D-*manno*-octulosonic acid 8-phosphate (KDO 8-P) synthase (K_i = 26 nM) [1], Dimethylarginine dimethylaminohydrolase (DDAH1, IC_{50} = 9 μM) [2] and was also described to be effective against hepatitis C virus (HCV, IC_{50} = 11 μM) and human immunodeficiency virus (HIV, IC_{50} = 1 μM) [3], although the target and mechanism of anti-viral action is not completely clear. Searching the Pubchem BioAssay Database revealed 7 other proteins (histone lysine methyltransferase G9a, cytochrome P450 2C9, hydroxysteroid (17-beta) dehydrogenase 4, 15-hydroxyprostaglandine dehydrogenase, human muscle pyruvate kinase, aldehyde dehydrogenase 1, 15-human lipoxygenase 2) that were affected by **1** with bioactivity values in the range from 0.11 to 14 μM [4]. **1** was inactive in 134 other bioassays. These findings, suggest a certain potential for unselectivity of benzothiazin-6-imines. However, with the exception of KDO 8-P synthase, the reported activities for mentioned proteins are primarily in the micromolar range. Very recently, our group discovered **1** as an exceptional potent inhibitor (IC_{50} = 11 nM) of human histone deacetylase 8 (HDAC8) and showed that it is highly selective against the human isoenzymes HDAC1-7 [5]. The most potent analog shows an IC_{50}-value of 2.9 nM against HDAC8. HDAC8 is an established target for T-cell lymphoma, childhood neuroblastoma and related to several other types of tumor [6]. Our finding was completely unexpected, since **1** lacks a classical zinc binding group that is a common feature of most known inhibitors of zinc-dependent HDACs. Moreover, the structure-activity relationship of analog compounds appeared to be very broad suggesting great potential for further optimization using medicinal chemistry methods [5]. Okazaki et al. reported that the distinct S-N bond in the isothiazolopyrimidine scaffold was immediately cleaved in the presence of GSH or other

reducing agents giving the thiophenol **3**, which was suggested to be the active anti-viral component [7]. Ghebremariam et al. observed that **1** is a long persistent inhibitor of DDAH and suggested that it may bind covalently to a cysteine residue in the catalytic site eventually forming the mixed disulfide **6** [2]. We also observed a long lasting inhibitory effect of **1** on HDAC8: About 90% of the enzyme remained inactive after 24 h dialysis. If the inhibitory mechanism involved covalent modification, what would explain the noteworthy selectivity for HDAC8 against other targets and even closely related HDAC isoenzymes? And what could be learned from the specific mode of action to develop optimized non-hydroxamate HDAC8 inhibitors? These considerations motivated us to study the inhibition mechanism of HDAC8 by **1** in great detail combining biochemical and biophysical methods with high-resolution HPLC-coupled ESI-MS / MS techniques.

2. Materials and methods

Materials. All reagents and solvents were purchased from Sigma, Fluka, Bachem, Roth or Tocris with a purity of 98% or higher. HPLC solvents were purchased from VWR with analytical grade or better. Sequencing grade modified Trypsin lyophilized was purchased at Promega. To minimize artificial oxidation of free thiols all measurements were performed in degassed buffer solutions. To prevent oxidation during storage, enzymes were stored in the presence of 1 mM TCEP. TCEP was removed immediately before measurements by GPC with Zeba Spin Desalting Columns 7K MWCO (Thermo Scientific).

Mutagenesis. Mutant HDAC8 variants were generated using splicing by overlap extension PCR (SOE-PCR) with the following Primers:

HD8_BamHI_rev: 5'-AGGTGGATCCTTAAACAACGTGCTTCAGATTGCC-3',

HD8_NdeI_for: 5'-GCGCATATGGAGGAGCCGGAGGAG-3',

HD8_C102S_for: 5'-GGGCTAGGTTATGACTCCCCAGCCACTGAAGGGATA-3',

HD8_C102S_rev: 5'-TATCCCTTCAGTGGCTGGGGAGTCATAACCTAGCCC-3',

HD8_C153S_for: 5'-GATGAAGCATCTGGTTTTTCTTATCTCAATGATGCT-3',

HD8_C153S_rev: 5'-AGCATCATTGAGATAAGAAAAACCAGATGCTTCATC-3'.

DNA sequencing was performed at the sequencing service at the LMU Munich with the cycle, clean and run (BigDye v3.1) protocol.

HDAC8 expression and purification. pET14b vector (Novagen, EMD Millipore) containing codon-optimized human HDAC8, fused to a His6 SUMO tag, was used to express HDAC8 in E. coli (BL21) DE3 pLysS. Cells were harvested by centrifugation for 10 min at 8000 g and 4 °C and resuspended in lysis buffer (pH 8.0) containing 150 mM KCl, 50 mM Tris, 5 mM imidazole, 5 mM DTT, 1 x HALT protease inhibitor cocktail (Thermo Scientific) and 5 µg/mL DNAseI. The cell suspension was sonicated and lysates were clarified by centrifugation at 18000 g for 30 min at 4 °C and sterile filtration. The filtrate was subsequently added to a 5 mL column volume of cOmplete His tag purification resin (Roche), equilibrated with IMAC buffer A (pH 8.0) containing 150 mM KCl, 50 mM Tris and 5 mM imidazole. After washing with 50 mL of the same buffer His6-SUMO-HDAC8 was eluted with IMAC buffer B (pH 8.0) containing 150 mM KCl, 50 mM Tris and 100 mM imidazole. Subsequently 10µg/ml His6 tagged SUMO-Protease was added to the eluted HDAC8 fusion protein. Cleavage of His6-SUMO tag occurred overnight whilst dialyzing against 25 mM Tris, 50 mM NaCl and 5 mM ß-ME (pH 8.0) at 4 °C. Then His6-

SUMO tag and SUMO-Protease was removed by a second IMAC with AIC buffer A (pH 8.0) containing 25 mM Tris and 50 mM NaCl and 5 mM imidazole. HDAC8 containing flowthrough was concentrated and further purified on a strong anion exchanger (Bio-Scale Mini Macro-Prep High Q 5 mL Cartridge, Biorad). After a washing step using AIC buffer A HDAC8 was eluted using AIC buffer B (pH 8.0) containing 25 mM Tris and 1 M NaCl. 5 mM DTT was added to prevent oxidation and remove possible ß-ME cysteine adducts. The final purification step included size exclusion chromatog-raphy with a HiLoad Superdex 75 material (GE) equilibrated with GPC Puffer (pH 8.0) containing 150 mM KCl and 50 mM Tris. The protein containing fractions were collected and concentrated. Glycerol and TCEP were added to final concentrations of 25 % and 1 mM and protein was stored at -20 °C. We typically obtained 3-5 mg HDAC8 from 1 liter culture.

Enzyme activity assay. All HDAC assays were executed in assay buffer (25 mM Tris-HCl pH 8.0, 50 mM NaCl and 0,001 % (v/v) pluronic F-68) in black half area 96-well microplates (Greiner Bio-One, Germany). 1 nM of $HDAC8_{WT}$ or 10 nM of HDAC8 mutants were preincubated with a serial dilution of the compounds for 1 h at 30 °C, before initiating the enzyme reaction by addition of 10 µM Boc-Lys(TFA)-AMC. Some enzyme/compound mixtures were treated with either 1 mM TCEP or various concentrations of GSH for 1h at 30 ^{0}C, before the enzyme reaction was started. The reaction was stopped after 60 min by adding 1.67 µM SATFMK. The deacetylated substrate was cleaved with 0.42 mg/mL Trypsin to release fluorescent AMC, which was detected with a microplate reader (PHERAstar FS, BMG LABTECH) with fluorescence excitation at 360 nm and emission at 460 nm. IC_{50} values were calculated by generating dose-response curves in GraphPad Prism 6 and fitting those to a 4-parameter fit model. Sirtuin assays were performed according to a published procedue [8].

Dialysis. HDAC8 (500 nM) was incubated with 100 µM **1** or buffer (control) for 1 h at room temperature and dialyzed (MEMBRA-CEL® dialysis membrane MWCO 3500, Serva, Germany) against 500-fold assay buffer with or without 50 mM ß-mercaptoethanol (β-ME) for 22 h at 4 °C. Samples were taken before and after dialysis to determine the activity of the protein, by adding 20 µM Boc-Lys(TFA)-AMC and incubating for 30 min at 30 °C. The reaction was stopped by the addition of 1.7 µM SATFMK and 0,42 mg/mL Trypsin. Free AMC was detected in a microplate reader with fluorescence excitation at 360 nm and emission at 460 nm.

Tryptic digestion. All tubes were cleaned with acetonitrile and water before use. 113 µM HDAC8 was treated with 300 µM **1** for 1 h at 25 °C in 10 mM ammonium bicarbonate buffer (ABC) while shaking at 400 rpm. A control sample was carried along without the addition of **1**. After treatment the samples were denatured at 90 °C for 30 min and alkylated with 14.5 mM iodoacetamide for 1h at room temperature in the dark. All samples were diluted with ABC buffer to 56.6 µM HDAC8 to accomplish a pH value between 7 and 8. Tryptic digestion was started with 28.6 µg/mL sequencing grade modified trypsin (Promega, Germany) at 37 °C for 18 h while shaking at 400 rpm. The digestion process was stopped by freezing and storing the samples at -20 °C immediate after digestion till measurement.

Quantitative HPLC/ESI-QTOF-MS/MS. The liquid chromatography tandem mass spectrometry (LC-MS/MS) system consisted of an Agilent 1100 high performance liquid chromatograph (HPLC) equipped with a micro vacuum degasser, Multospher 120 RP 18-AQ, 250 x 4 mm (i.d.), 5 µm particle size coupled to an ABSciex X500R QTOF mass spectrometer equipped with an IonDrive TurboV ESI-source. HPLC separation was performed under gradient conditions with mobile phases of acetonitrile + 0.1% (v/v) formic acid (A) and Water + 0.1% (v/v) formic acid (B) at a flow rate of 0.5 mL/min. The gradient condition was set as follows: 0-5

min 10% A, 5-20 min linear increase to 70% A, 20-25 min 70% A, 25-26 min linear decrease to the initial condition of 10% A, 26-35 min 10% A for column equilibration. The injection volume was 10 µL. The parameters used for ESI-QTOF-MS/MS analysis in positive ion mode were as follows: nebulizer (gas 1), 50 arbitrary units; turbo gas (gas 2), 55 arbitrary units; curtain gas, 35 arbitrary units; source temperature, 500°C; ionspray voltage + 5.5 kV, declustering potential (DP), 50 V; collision energy (CE), 10 V. TOF MS full scan and product ion Data were acquired by information dependent acquisition (IDA) scan mode in the mass range of 100-700 Da. The calibration delivery system (CDS) was set to perform an automatic external calibration every ten samples. Data acquisition and processing was performed with the Sciex OS 1.3 software.

The same system and mobile phases were used for peptide analysis but with different conditions as mentioned before. A 100 x 2 mm (i.d.), 2.3 µm particle size TSKgel Super-ODS C18 column with a flow rate of 0.2 mL/min was used with the gradient conditions set as follows: 0-5 min 5% A, 5-40 min linear increase to 80% A, 40-45 min 80% A, 45-55 min linear decrease to 5 % A and 55-60 min 5 % A for equilibration. The injection volume was 10 µL. ESI-QTOF-MS/MS parameters were as follows: gas 1, 45 arbitrary units; gas 2, 45 arbitrary units; curtain gas, 35 arbitrary units; source temperature, 400°C; ionspray voltage + 5.5 kV, DP, 50 V; CE, 10 V. For data acquisition IDA scan mode was used in the mass range of 450-2000 Da. Dynamic collision energy mode was set active.

The software for Theoretical fragmentation and peptide fragment assignment were integrated in Sciex OS 1.3.

Protein crystallography. Protein expression and crystallization of HDAH was performed as described previously [9, 10]. Briefly, crystals of HDAH were grown by hanging drop vapor

diffusion against 500 µl reservoir, the reservoir solution contained 0.1 M malate-imidazole buffer (pH 5.25) and 3-6% PEG400. The reservoir solution and protein (10 mg/ml) were mixed in a 1:1 ratio to a final volume of 4 µl. Crystals grew in three to ten days at 20°C. The obtained crystals of HDAH were soaked by adding of 2µl of a 2 mM compound **1** dissolved in the reservoir solution directly to the drop and incubated for 24h. Cryo-protection was achieved by washing the crystal in 0.1 M malate-imidazole buffer with a pH of 5.25 and 30% PEG400. The cryoprotected crystals were flash frozen in liquid nitrogen. Diffraction data were collected at 100 K on beamline PXII at the Swiss Light Source (SLS, Villigen, Switzerland).

Global fit analysis of reaction kinetics. The time courses of the relative concentrations of molecular species **1-9** were obtained from quantitative ESI-MS-measurements as described above. The simulation and modeling program COPASI was used to fit eligible models of the reaction mechanism to the set of time resolved concentrations [11]. In short, the model is described by a system of ordinary differential equations, which is determined by kinetic rate constants. These parameters were optimized by starting with randomized start values for all parameters and minimizing the total error sum of squares for the entire set of data curves by subsequently application of the implemented Evolution Strategy, Evolutinary Programming and Levenberg-Marquardt-algorithms. To estimate the absolute concentrations from relative concentrations, proportional factors were concurrently fitted to the data. Entering the determined rate constants and proportional factors into the model allowed for the simulation of time-courses of all molecular species involved in the complex reaction mechanism.

Molecular docking. Modeling, preparation and visualization of structural data as well as molecular docking was performed using MOE 2016 software (Chemical Computing Group ULC,

Canada). At first crystal structure data PDB-ID 1T64, 1T69, 1VKG, 3SFF representing significant conformations of HDAC8 in complex with various inhibitors were loaded into the program and subjected to structure preparation including 3D protonation for subsequent docking. The partial charges of all protein and ligand atoms were calculated using the implemented Amber12 force field. Molecular docking was performed choosing the triangle matcher for placement of the ligand in the binding site and ranked with the London dG scoring function. The best 30 poses were passed to the refinement and energy minimization in the pocket using the induced fit method and then rescored with the GBVI/WSA dG scoring function.

3. Results and discussion

3.1. *Compound **1** and closely related analogs show similar activity against HDAC8*

1 been recently described as a novel, potent, and selective lead structure for $HDAC8_{wt}$ inhibitors [5]. Most interestingly, the compound contains no common zinc-chelating group characteristic for most HDAC inhibitors. Particularly the prevention of the ubiquitous hydroxamate group with a high potential for unspecific zinc ion binding and suspected mutagenicity let the pharmacophor of **1** appear an attractive alternative to existing HDAC8 inhibitors [12]. In light of its novel structure highly dissimilar to known HDAC inhibitors, we wondered about the mode of action of compound **1**. Since **1** was reported to exhibit anti-viral properties, Okazaki et al. investigated the chemical stability of the compound in greater detail and found out that **1** decomposes in the presence of glutathione (GSH) into thiophenol **3** which was believed to be the active anti-viral substance [7]. We confirmed the chemical instability of **1** in the presence of GSH, but besides **3** we also found considerable amounts of **5**, **6**, **8** and **9** using high-resolution ESI-MS. Next, we noticed that thiophenol **3** decomposes into sulfenamide **5** and thiourethane **8** immediately after dissolvation in 10 mM ammonium carbonate buffer (pH 8.0) (Fig. S1). To identify the active substance that inhibits $HDAC8_{wt}$, we determined IC_{50}-values for analogs **1**, **3** and **5**, freshly dissolved in assay buffer (Fig. 1A). Surprisingly, all three compounds turned out to be similarly potent against $HDAC8_{wt}$ showing IC_{50}-values of about 1 nM (Tab. S1). To simplify the reporting of next results, we will talk about HDAC8 inhibition by **1** when this compound is added to the enzyme, knowing that **1** can decompose into **3** and **5** in the presence of thiol groups such as those in the side chain of solvent-accessible cysteines at the surface of HDAC8.

3.2. *Inhibition of HDAC8 is mediated by covalent modification of at least one cysteine*

Since **1** inhibits in the concentration range of applied $HDAC8_{wt}$, its binding is supposed to be very tight. To distinguish between a covalent and a reversible binding mode, we performed a dialysis of the complex formed by the interaction of HDAC8 and compound **1** (Fig. 2). After 22 hours of dialysis in the absence of reducing agent, the enzyme activity of $HDAC8_{wt}$ remains substantially inhibited. In contrast, HDAC8 activity is completely recovered, if the protein-ligand complex is dialyzed against buffer including β-ME. This suggests covalent modification of $HDAC8_{wt}$ by **1** involving the formation and fission of a disulfide bridge between at least one accessible cysteine of the enzyme and the inhibitor. This conclusion is supported by the loss of activity of compounds **1**, **3** and **5** in the presence of the reducing agent TCEP that breaks disulfide bonds (Fig. 1B, Tab. S1). Moreover, addition of TCEP to preformed complexes between **1**, **3** and **5** and $HDAC8_{wt}$ reverses enzyme inactivation confirming the reversibility of the inhibitory mechanism that involves the formation and disruption of disulfide bonds. It should be noted that GSH at concentrations up to 1 mM is not able to reverse the inactivation of $HDAC8_{wt}$ once the disulfide with **1** is formed, possibly due to a less negative redox potential of GSH (-230 mV compared with -290 mV of TCEP) (Tab. S1).

*3.3. Mechanism of GSH-modification by **1***

The reaction of GSH and **1** was investigated previously to learn about the corresponding transformations in aqueous solution. Okazaki et al. found that **1** was immediately cleaved in the presence of GSH producing **3** [7]. Similar to our results, **1** and **3** showed comparable EC_{50}-values for the inhibition of HIV-1 infection. From these results, **1** was suggested as prodrug for the

bioactive thiophenol **3** [7]. We applied the powerful technique of high-resolution ESI-MS to prove the existence of nine occurring molecular species in the reaction of GSH and **1** (Fig.'s 3, S2, S3, S5 and S6). In contrast to Okazaki, we verified only very small amounts of **3** immediately after mixing **1** and GSH. Similarly, purified **3** also disappears instantly after dissolvation in ammonium carbonate buffer pH 8.0 generating significant amounts of sulfenamide **5** and only minor amounts of **9** (Fig. S1). Therefore, we conclude that **3** is chemically unstable in aqueous solution. The concentration of every proven molecular entities involved in the reaction between GSH and **1** was quantified using LC-ESI-MS, and the corresponding time courses analyzed during a period of 15 h to elucidate the accurate mechanism of this unexpected complex reaction (Fig. 4 A, B). The decay of **1** shows two phases: a rapid drop within the first hour of reaction and a slow decrease over hours. In contrast, GSH disappears completely from the mixture within 30 minutes. Two intermediates, **5** and **6** are generated rather rapidly reaching their peak concentration at about 2 h and 0.5 h, respectively. While the mixed disulfide **6** vanishes after 3 h, the sulfenamide **5** is unexpected metastable and still present as one of the dominating species after 15 h. GSSG appears in conjunction with the rapid drop in GSH concentration and subsequently decreases slowly approaching a rather stable level. The occurrence of glutathione-thiocyanate **(4)** was unequivocally proven by ESI-MS/MS data (Fig. S2,S3), removal of the cyano group and the characteristic formation of a cyclic thiazolamine after reacting with a 5-fold excess concentration of cysteine (Fig. S4). Interestingly, **4** was shown to arise rapidly and be chemically stable for at least 15 h (Fig. 4A). Simulations suggest that cyanylation is the predominant modification of GSH compared with disulfide formation (Fig. 4B). The whole complex reaction is superimposed by slowly emerging **8** and

sulfinic acid **9** as final products. The array of time-dependent concentrations of all species was fit to a model taking all experimentally verified molecular entities into account (Fig. 4C).

The entire set of experimental time-dependent concentrations is well described by the reaction scheme in Fig. 4C). Comprehensive data analysis using COPASI provides the rate constants for every depicted elementary reaction steps (Tab. S2). The reaction mechanism postulates the formation of glutathione thiocyanate, **4**, proven be ESI-MS/MS, as suggested by Ghebremariam for the covalent inactivation of DDAH1 [2]. In the same step thiophenol **3** is generated that is instantly oxidized (see above) giving the central metastable sulfenamide **5**. The mixed disulfide **6** generated from **5** can react further with GSH giving GSSG and **3**. When GSH is consumed, the chemical equilibrium between **5**, **6** and **7** is established leading to a progressive drop in the concentration of **6** that is no longer produced from **5** and a slower moderate decrease of GSSG concentration. Simultaneously, two slow side reactions take place generating two chemically stable final products: Metastable **5** is oxidized to sulfinic acid **9**, and residual **1** is hydrolyzed to thiourethane **8**. The comprehensive analysis of quantitative and time-resolved data provide substantial insight into the accurate mechanism by which model compound GSH and **1** react. From these results we conclude that **1** is a general dual cysteine modifier in aqueous solution that can transfer cyano groups to thiol residues and also produces mixed disulfides between cysteines and thiophenol **3**.

3.4. *Covalent modification of HDAC8$_{wt}$ by **1***

In an attempt to elucidate the accurate binding mode of **1** to HDAC enzymes we tried to crystallize complexes of **1** with HDAC8 and HDAH, a bacterial homolog that crystallizes nicely in our hands [9, 10]. We added **1** to a HDAH crystal in order to soak the ligand into the binding pocket. Unfortunately, we were not successful to obtain crystals of the HDAC8 complex with

sufficient quality for structure determination. But we were able to determine the structure of the reaction product of HDAH and **1** at a very high spatial resolution of 1.47 Å. To our surprise, the binding site pocket was unoccupied. Instead, we found covalent modifications of two cysteines (C51 and C295) at the surface of HDAH.

Although no reducing agent was present during crystallization, both modifications were clearly visible as mixed disulfides between the respective cysteine and thiophenol **3** as shown exemplary for C51 (Fig. 5). The observed modifications of HDAH are in agreement with the reaction mechanism between **1** and GSH (Fig. 4C), which has been elucidated on the basis of quantitative ESI-MS data. The cysteine modification reaction seems to be rather unspecific and is supposed to be a common mechanism for unselective inhibition of other enzymes, if functional cysteines are hit.

To identify putatively modified cysteines in $HDAC8_{wt}$, a reaction mixture of $HDAC8_{wt}$ and **1** was subjected to tryptic digestion followed by LC-ESI-MS/MS analysis. In fact, C153 in the catalytic site as well as various other cysteine residues were modified by **1** (Tab. S3). Five cysteines, including C28, C153, C244, C314 and C352 showed cyanylation upon treatment with **1** (Fig. S3). These modifications are in agreement with the unspecific affinity labeling mechanism of GSH. Since the reaction of $HDAC8_{wt}$ with **1** was performed at high concentrations of almost four orders of magnitude above the IC_{50}-value of **1**, only qualitative statements about the modified cysteines in $HDAC8_{wt}$ and no assessment of a preference for a particular cysteine can be made. However, it appears plausible that the effect of **1** or **5** responsible for the inhibition of $HDAC8_{wt}$ is mainly due to the modification of C153 in the catalytic site pocket thereby permanently blocking access to the catalytic center. In any case, **1** and most likely also related benzothiazine-imines are clearly able to modify solvent accessible thiol groups on protein

surfaces and produce cysteine-thiocyanates as well as mixed disulfides between cysteine and **3**. For the majority of enzyme targets including other HDAC isoenzymes that are effected by **1** only moderate activities in the micromolar range have been reported [2-5]. **1**, **3** and **5** were also tested against Sirtuins, because Sirt1 was shown to respond to similar inhibitors [13]. The compounds show moderate micromolar activities against Sirt1 and Sirt2, but were virtually inactive against Sirt 3 (Tab. S7). This is in agreement with moderate activity on a variety of protein targets and our finding that **1** is a general cystein modifier. Most recently, thiol reactive histone acetyltransferase (HAT) inhibitors have been considered as essentially nonselective interference compounds [13]. Typically, these HAT inhibitors show moderate IC_{50}-values in the micromolar range. However, CPTH2, a thiol-reactive HAT (GCN5) inhibitor, does not inhibit HDAC8 (IC_{50} > 50 μM, Fig. S13). Despite its unspecific cysteine reactivity, **1** is highly potent and selective against HDAC8 with an IC_{50}-value of 11 nM [5]. Since C153 is conserved among all human HDAC isoenzymes and other cysteins in HDAC8 are also modified, another component had to be the major contributor to the observed selectivity of compound **1**.

3.5. *C102 and C153 are involved in the inhibition mechanism of HDAC8*

Looking at available crystal structures of HDAC8 (e.g. PDB-ID: 1T69) reveals C153 in the active site and C102 in close proximity to be eligible for a potential chemical modification by **1**. In the following, single mutants $HDAC8_{C102S}$ and $HDAC8_{C153S}$ and the double mutant $HDAC8_{C102S/C153S}$ were produced to elucidate the participation of the exchanged cysteines in the mechanism of inhibition. Since all HDAC8 variants were enzymatically active, the inhibitory efficacy of compounds **1**, **3** and **5** could be determined in terms of IC_{50}-values (Fig. 1A, Fig. S12). To demonstrate the reversibility of a putative disulfide bond involving C102 or C153,

respectively, the concentration series were performed in the absence or after the addition of 1 mM TCEP to the preformed complex between HDAC8-variant and compound (Fig. S12). After the addition of the reducing agent, the enzyme activity of all HDAC8 variants is recovered confirming that the mechanism of HDAC8 inhibition by **1** and derivatives thereof involves the formation of disulfide bonds (Fig. S12). SAHA was used as control that shows absolutely no susceptibility to reducing agent TCEP. IC_{50}-values of SAHA varied slightly between 0.29 and 2.4 μM among the 4 HDAC8 variants (Tab. S1). While SAHA behaves like a classical active site inhibitor against the double mutant $HDAC8_{C102S/C153S,}$ compounds **1**, **3** and **5** show a biphasic dose-response curve against the same enzyme (Fig. S12G). This finding suggests an allosteric interaction site at this HDAC8 variant. The IC_{50}-values of **1**, **3** and **5** for the more potent site is comparable with the IC_{50}-values against the single mutants of HDAC8. We hypothesize that other solvent accessible cysteines at the surface of HDAC8 may react with analogs of **1** enabling an indirect modulation of the catalytic efficiency of $HDAC8_{C102S/C153S}$, which is not capable of full enzyme inactivation. Only at very high concentration of **1**, **3** or **5** (> 10 μM) full inhibition is achieved probably by additional unselective modifications of the HDAC8 variant. These results suggest that HDAC8 contains at least two types of interaction sites: A high affinity site involving cysteins C102 and C153 in close proximity to the active site and at least one low affinity allosteric site where unselective disulfide modification can take place at higher concentrations of **1** analogs. There are only rather small differences in IC_{50} values of **1**, **3** and **5** between $HDAC8_{wt}$ and $HDAC8_{C153S}$ and $HDAC8_{C102S}$ (Tab. S1). Due to the low enzyme activity of the HDAC8 mutant proteins as much as 10 nM enzyme concentration was chosen to measure and compare the dose-response curves of the inhibitors against all HDAC8 variants. Since particularly the IC_{50}-values with $HDAC8_{wt}$ approach the level of enzyme concentration, these IC_{50}-values only

represent upper limits of the true inhibitory activity. This is also recognizable by the distinct steep shape of the dose-response curves of **1**, **3, 5** on $HDAC8_{wt}$ indicating nearly stoichiometric tight binding of a ligand (Fig. S12 A). Nevertheless, a clear differentiation between the inhibition of $HDAC8_{wt}$ and the mutant enzymes is not possible on the basis of these data. Unfortunately, it is not possible to lower the enzyme concentration of the mutant variants because of their weak enzyme activity. Moreover, it is more conclusive to investigate the inhibition kinetics of covalent inactivators such as cystine modifiers. In fact, the inhibition kinetics of $HDAC8_{wt}$ by **1** is clearly different from that of the mutant variants (Fig. 6). $HDAC8_{wt}$ is essentially completely inhibited after 2 minutes in striking contrast to $HDAC8_{C102S}$, $HDAC8_{C153S}$ and $HDAC8_{C102S/C153S}$ indicating the pivotal role of both cysteins in the inhibition mechanism. **1** shows a slow inhibition of the double mutant HDAC8 approaching an equilibrium level of about 50% residual enzyme activity, which is in agreement with the corresponding dose-response curve (Fig. S12G). This finding suggests that the inhibition mechanism does not involve a continuing chemical inactivation but is rather maintained by non-covalent binding. In contrast, inhibition of $HDAC8_{C153S}$ and $HDAC8_{C102S}$ does not reach equilibrium but still continues even after 30 min of reaction suggesting a covalent modification of C102 and C153 (Fig. 6). Interestingly, C102 seems to be more rapidly hit by **1** than C153. The enzyme activity of $HDAC8_{C153S}$ drops instantly by about 50% and than shows a slow ongoing inhibition, whereas $HDAC8_{C102S}$ shows only the slow inhibition kinetics. The differential inhibition kinetics of the HDAC8 variants clearly demonstrates, that the presence of both cysteins, C102 and C153, is required for the rapid inhibition mechanism of $HDAC8_{wt}$.

3.6. *Non-covalent molecular recognition of **1** and **5** by $HDAC8_{wt}$*

The reactivity of **1** in the presence of GSH and the unselective modification of many proteins render benzothiazine-imines unsuitable for therapeutic applications. On the other hand, the significant increase in potency of **1** against HDAC8 by three orders of magnitudes cannot be explained by simple nonspecific affinity labeling. Therefore, we hypothesize that the experimentally observed high selectivity of benzothiazine-imine analogs for HDAC8 is caused by an additional specific contribution to inhibition such as a beneficial non-covalent molecular recognition in the active site or another transient binding pocket that precedes covalent modification. Our hypothesis is supported by the inhibition kinetics of the HDAC8$_{C102S/C153S}$ double mutant that is in agreement with non-covalent binding (Fig. 6). The presumed non-covalent molecular recognition of **1** and **5** by HDAC8 was investigated further using computational methods, particularly molecular docking. It is known that the conserved binding pocket of HDAC8 is highly conserved among members of the HDAC family. However, HDAC8 is very special with respect to enhanced malleability of the region around the classical active site. There exist various X-ray structures that demonstrate the considerable flexibility of HDAC8 and a transition from closed (PDB-ID: 1T69) to sub-open (PDB-ID: 1T64) to wide-open (1VKG) binding pockets [14]. Most remarkable, the sub-open state shows a deep second binding pocket next to the conserved one, which is occupied with a second inhibitor molecule. The L1-and L2-loop are primarily responsible for ligand-induced conformational changes in HDAC8 [14-16]. Both loops display highly varying amino acid compositions in HDAC1 and HDAC8. In addition, the L1-loop of HDAC1 is 5 amino acids longer than that of HDAC8 causing a different flexibility profile in both isoenzymes [17]. Compounds **1** and **5** were docked into the binding pockets of above mentioned representative HDAC8 structures to determine the favored binding modes and identify putative beneficial contacts. Furthermore, **1** was also docked into available

crystal structures of HDAC isoenzymes HDACs 1, 2, 4 and 6 to understand the observed selectivity in enzyme activity assays on a molecular basis (Fig. S9). The best docking score is obtained for HDAC8, thus confirming the experimental data (Tab. S4).

Docking of **1** into various crystal structures of HDAC8 revealed clearly different scores indicating different affinities to distinct conformations of HDAC8 (Tab. S5). The best docking pose of **1** at the bottom of the active site pocket in HDAC8 (PDB-ID: 1T69) is shown in Fig. 7A. A comparison of the docking result between HDAC8 (PDB-ID: 1T69) and **1** with the crystal structure of HDAC8 bound to an amino-acid inhibitors (PDB-ID: 3SFF) shows a substantial overlap of both inhibitors binding to the transition area between the acetyl-lysine binding tunnel and the acetate release channel (Fig. 7B). The best docking pose of **1** in HDAC1 (PDB-ID: 5ICN) is located in the conserved active site binding pocket (Fig. S9). The closest distance between carbon atoms of F150 (matching F152 in HDAC8) and Y303 (matching Y306 in HDAC8) is 4.0 Å impeding access to the acetate release channel (Fig. S10). In addition, M30 located in the L1-loop of HDAC1 intrudes into the acetate release channel and clashes with superimposed compound **1** docked to HDAC8. In contrast, F152 and Y306 in the docked complex between HDAC8 and **1** are moved to the side allowing the aromatic moiety of **1** to protrude into the acetate release channel similar to the amino-acid derived inhibitors of Whitehead et al. [18] (Fig. 7 and S10). The dominating molecular interactions between HDAC8 and **1** are zinc binding through the imine nitrogen of **1** and a hydrogen bond between a nitrogen atom of the tetrahydropyrimidine ring of **1** and Y306. These are complemented by a cation-π-interaction between the aromatic ring of **1** and R37 and mainly hydrophobic interactions to F152, F208, C153, I34 and G304. The aromatic ring of **1** forms a π-π T-shaped interaction with W141 (Fig. S10). Acetate release is believed to be mediated by R37 stabilizing the charge of acetate in

cooperation with W141 relocating its indole moiety to close the release channel [18, 19]. The pivotal W141 is substituted by leucine in class I HDACs 1, 2 and 3, and has no counterpart in class II HDACs. This amino acid difference in the acetate release channel and also in the L1-loop (e.g. M30 in HDAC1 and 2 intrudes into the acetate release channel) as well as in the L2-loop are supposed to have significant impact on HDAC8 flexibility and the geometry of the internal binding cavity. In summary, differences in pivotal amino acids, protein malleability and the particular binding mode of **1** to HDAC8 is suggested to be the reason for the observed selectivity for HDAC8 and against class I HDACs 1 and 2 as well as class IIa HDAC4 and class IIb HDAC6. Once **1** is non-covalently bound to HDAC8, it is brought in close proximity to C153 lining the active site pocket (Fig. S10) and is supposed to have an increased probability to cyanylate this cysteine (Fig. 8). The released thiophenol **3** is rapidly oxidized to **5** in free solution. But in principle **3** could also remain transiently bound and stabilized by non-covalent interactions before reacting further with the adjacent C153-thiocyanate (Fig. 8). The sulfur atom of the thiocyanate possesses an electrophilic character due to the cyano moiety acting as a leaving group [20]. The experimentally observed mixed disulfide can be reached by substituting the cyanyl group by thiophenol **3**.

Docking **3** into HDAC8 with cyanylated C153 shows that **3** is well accommodated in the binding pocket and has a short distance of 4.7 Å between the thiol group and the sulfur atom of C153 (Fig. S7). During the first hour of interaction between **1** and GSH the next prominent reactive intermediated during the reaction with thiol agents is the sulfenamide **5** which is rapidly formed by oxidation of **3** and rather stable under assay conditions. In fact, **5** showed similar potency against HDAC8 than **1**. Therefore, non-covalent binding of **5** followed by direct conversion of C153 to the mixed disulfide with **3** could be an alternative pathway to inhibition of HDAC8

according to the model reaction between GSH and **1** (Fig. 8). Docking of **5** to HDAC8 revealed a binding mode, where a partially negatively charged nitrogen of **5** binds closely to the zinc ion (Fig. S8). The non-covalent interaction is enhanced by a hydrogen bond to Y306 and various hydrophobic interactions to C153, W141, H142, H143, F208, M274, Y306 and G304. The thiol group of C153 and the sulfur atom of **5** are brought in proximity (4.8 Å) allowing for a subsequent modification reaction (Fig. S8, Tab. S4). Since ESI-MS/MS data prove the cyanylation of C153, we conclude that the interaction between **1** and HDAC8 follows the cyanylation pathway (Fig.8 upper panel). However, since **1** is not so stable in aqueous solution and **5** is also capable to inhibit HDAC8 with comparable potency, we cannot rule out the second pathway which starts with the interaction between metastable **5** and HDAC8 producing a mixed disulfide that blocks access to the active site (Fig. 8 lower panel).

4. Conclusions

The benzothiazine-imine **1** is a potent and selective inhibitor of HDAC8 with an unprecedented chemical scaffold lacking traditional zinc binding groups. This study provides detailed insight in the reaction mechanism of **1** with GSH on the basis of quantitative and time-resolved ESI-MS/MS data. Compound **1** is chemically not stable in the presence of GSH. The reaction produces thiocyanate and disulfide modifications of GSH, GSSG as well as a mixed disulfide with **3**. Surprisingly, the sulfenamide **5** appears to be relatively stable over the course of 15 h at pH 8.0.

Combined MS, biochemical and crystal structure data of the interaction of HDAC8 with **1** provide clear evidence that 1) **1** is a covalent inhibitor of HDAC8, 2) inhibition is reversible in the presence of reducing agents, 3) C153 in the active site and adjacent C102 are involved in the inhibition mechanism and 4) **1** modifies various cysteines in HDAC8 forming either thiocyanates or mixed disulfides with **3**.

The reactive nature of **1** is obviously the cause for its moderate inhibitory effects against several other targets. However, the single-digit nanomolar potency and high selectivity of **1** for HDAC8 even against closely related HDAC isoenzymes requires a further important component in the specific recognition of **1** by HDAC8.

On the basis of molecular docking results we propose putative selective non-covalent binding of **1** and **5** to HDAC8 prior to covalent modification. The optimal binding mode of **1** at the bottom of the active site protrudes into the acetate release channel showing distinct amino acid differences to other HDAC isoenzymes. The close proximity of **1** and C153 within the active site pocket is supposed to accelerate the covalent inactivation particularly in HDAC8 and is proposed to be a major determinant for the observed selectivity.

It is quite clear, that the reactive nature of **1** and its analogs render them unsuitable for therapeutic treatment. However, it appears attractive to further examine the specific molecular recognition motif of **1** that utilizes the transition area between the catalytic site and acetate release channel. We are currently pursuing several strategies towards less reactive variants of **1** that exploit the specific non-covalent molecular recognition of this class of compounds by HDAC8.

Conflict of interest

The authors declare no competing financial interest.

Acknowledgement

NW and MJ thank the Deutsche Forschungsgemeinschaft (DFG,

Ju295/14-1) for funding.

Appendix A. Supplementary data

Figure Captions:

Fig. 1: Dose-response curve of **1**, **3**, **5** and control SAHA against indicated $HDAC8_{wt}$. 1 nM $HDAC8_{wt}$ was A) in the absence and B) in the presence of TCEP incubated with varying concentrations of indicated inhibitor for 1 h at 30 °C. The remaining $HDAC8_{wt}$-acitivity was determined using the standard enzyme activity assay. All data points represent means and standard deviations from 3 independent experiments. Solid lines are best-fit to a 4-parameter logistic.

Fig. 2: Irreversible binding of **1** to $HDAC8_{wt}$ becomes reversible upon addition of reducing agent β-mercapto ethanol (β-ME). Enzyme activity is referred to 100 % free $HDAC8_{wt}$. After addition of 100 µM **1** to 500 nM $HDAC8_{wt}$ the enzyme is completely inhibited (before dialysis). After 24 h dialysis at 4^0C in the absence of β-ME only weak and in the presence of 50 mM β-ME almost the entire enzyme activity is recovered. Shown data are means and standard deviations of three independent experiments.

Fig. 3: Quantitative ESI-MS of all observed educts, intermediates and products of the reaction between compound **1** and GSH (**2**). The bold numbers under the m/z ratios correspond to those in Fig. 4 of the main text. The spectra are measured after indicated time periods.

Fig. 4: A) Time courses of indicated species during the reaction between 2.3 µM **1** and 1.6 µM GSH in 10 mM ammonium carbonate buffer pH 8.0 at (26 ± 1) °C. Experimental relative concentrations as determined from ESI-MS. Solid lines represent a simultaneous fit of the reaction mechanism shown in C) to the data using COPASI. B) Simulated absolute concentrations on the basis of the reaction mechanism and rate constants determined in C) using COPASI. C) Proposed reaction mechanism of **1** with glutathione (GSH). GSSG is oxidized GSH

and **4** is glutathione-thiocyanate. All chemical species have been identified and quantified using ESI-MS (Fig. S2).

Fig. 5: Covalent modification of C51 in a crystal structure of HDAH (PDB-ID: 6GJK) after reaction with **1**. C51 forms a mixed disulfide bridge with thiophenol **3**. The blue mesh shows the $2F_o$-F_c-electron density map of the compound contoured at 1 sigma.

Fig. 6: Inhibition kinetics of different HDAC8 variants by compound **1**. 100 nM of the respective HDAC8 variant was incubated with 500 nM of freshly dissolved inhibitor at 30^0C. The residual enzyme activity was measured after varying incubation time periods. The data represent mean and standard deviation of at least four independent experiments.

Fig. 7: Docking of **1** into the active site pocket of HDAC8 (PDB-ID: 1T69). A) **1** binds at the bottom of the active site pocket and protrudes into the acetate release channel. The green dashed line indicates a hydrogen bond to Y306 and the magenta dashed line a metal-binding interaction between the imine group and the catalytic zinc ion. B) Overlay of **1** (orange) docked into PDB-ID 1T69 and the complex between HDAC8 and amino-acid based inhibitor (PDB-ID: 3SFF, green) [18]. Both compounds show pronounced overlap, particularly in the transition area between the acetyl-lysine binding tunnel and the horizontal acetate release channel.

Fig. 8: Two pathways of covalent modification at C153 in the active site of HDAC8 by **1** or **5** resulting in thiocyanate or mixed disulfide, respectively.

References

[1] M.R. Birck, T.P. Holler, R.W. Woodard, Identification of a Slow Tight-Binding Inhibitor of 3-Deoxy-d-m anno-octulosonic Acid 8-Phosphate Synthase, J. Am. Chem. Soc., 122 (2000) 9334-9335.
[2] Y.T. Ghebremariam, D.A. Erlanson, J.P. Cooke, A novel and potent inhibitor of dimethylarginine dimethylaminohydrolase: a modulator of cardiovascular nitric oxide, J. Pharmacol. Exp. Ther., 348 (2014) 69-76.
[3] A.M. Chamoun, K. Chockalingam, M. Bobardt, R. Simeon, J. Chang, P. Gallay, Z. Chen, PD 404,182 is a virocidal small molecule that disrupts hepatitis C virus and human immunodeficiency virus, Antimicrob. Agents Chemother., 56 (2012) 672-681.
[4] National Center for Biotechnology Information. PubChem Compound Database; CID=6603967, https://pubchem.ncbi.nlm.nih.gov/compound/6603967 (accessed Apr. 21, 2018). in.
[5] A. Kleinschek, C. Meyners, E. Digiorgio, C. Brancolini, F.J. Meyer-Almes, Potent and Selective Non-hydroxamate Histone Deacetylase 8 Inhibitors, ChemMedChem, 11 (2016) 2598-2606.
[6] A. Chakrabarti, J. Melesina, F.R. Kolbinger, I. Oehme, J. Senger, O. Witt, W. Sippl, M. Jung, Targeting histone deacetylase 8 as a therapeutic approach to cancer and neurodegenerative diseases, Future medicinal chemistry, 8 (2016) 1609-1634.
[7] S. Okazaki, S. Oishi, T. Mizuhara, K. Shimura, H. Murayama, H. Ohno, M. Matsuoka, N. Fujii, Investigations of possible prodrug structures for 2-(2-mercaptophenyl) tetrahydropyrimidines: reductive conversion from anti-HIV agents with pyrimidobenzothiazine and isothiazolopyrimidine scaffolds, Org. Biomol. Chem., 13 (2015) 4706-4713.
[8] B. Heltweg, J. Trapp, M. Jung, In vitro assays for the determination of histone deacetylase activity, Methods, 36 (2005) 332-337.
[9] C. Meyners, A. Kramer, O. Yildiz, F.J. Meyer-Almes, The thermodynamic signature of ligand binding to histone deacetylase-like amidohydrolases is most sensitive to the flexibility in the L2-loop lining the active site pocket, Biochim. Biophys. Acta, 1861 (2017) 1855-1863.
[10] C.E. Weston, A. Kramer, F. Colin, O. Yildiz, M.G. Baud, F.J. Meyer-Almes, M.J. Fuchter, Toward Photopharmacological Antimicrobial Chemotherapy Using Photoswitchable Amidohydrolase Inhibitors, ACS Infect Dis, 3 (2017) 152-161.
[11] S. Hoops, S. Sahle, R. Gauges, C. Lee, J. Pahle, N. Simus, M. Singhal, L. Xu, P. Mendes, U. Kummer, COPASI--a COmplex PAthway SImulator, Bioinformatics, 22 (2006) 3067-3074.
[12] S. Shen, A.P. Kozikowski, Why Hydroxamates May Not Be the Best Histone Deacetylase Inhibitors-What Some May Have Forgotten or Would Rather Forget?, ChemMedChem, 11 (2016) 15-21.
[13] J.L. Dahlin, K.M. Nelson, J.M. Strasser, D. Barsyte-Lovejoy, M.M. Szewczyk, S. Organ, M. Cuellar, G. Singh, J.H. Shrimp, N. Nguyen, J.L. Meier, C.H. Arrowsmith, P.J. Brown, J.B. Baell, M.A. Walters, Assay interference and off-target liabilities of reported histone acetyltransferase inhibitors, Nature Communications, 8 (2017) 1527.
[14] J.R. Somoza, R.J. Skene, B.A. Katz, C. Mol, J.D. Ho, A.J. Jennings, C. Luong, A. Arvai, J.J. Buggy, E. Chi, J. Tang, B.C. Sang, E. Verner, R. Wynands, E.M. Leahy, D.R. Dougan, G. Snell, M. Navre, M.W. Knuth, R.V. Swanson, D.E. McRee, L.W. Tari, Structural snapshots of human HDAC8 provide insights into the class I histone deacetylases, Structure, 12 (2004) 1325-1334.

[15] M. Brunsteiner, P.A. Petukhov, Insights from comprehensive multiple receptor docking to HDAC8, J. Mol. Model., 18 (2012) 3927-3939.
[16] D.P. Dowling, S.L. Gantt, S.G. Gattis, C.A. Fierke, D.W. Christianson, Structural Studies of Human Histone Deacetylase 8 and Its Site-Specific Variants Complexed with Substrate and Inhibitors, Biochemistry, 47 (2008) 13554-13563.
[17] N. Deschamps, C.A. Simões-Pires, P.-A. Carrupt, A. Nurisso, How the flexibility of human histone deacetylases influences ligand binding: an overview, Drug Discov. Today, 20 (2015) 736-742.
[18] L. Whitehead, M.R. Dobler, B. Radetich, Y. Zhu, P.W. Atadja, T. Claiborne, J.E. Grob, A. McRiner, M.R. Pancost, A. Patnaik, W. Shao, M. Shultz, R. Tichkule, R.A. Tommasi, B. Vash, P. Wang, T. Stams, Human HDAC isoform selectivity achieved via exploitation of the acetate release channel with structurally unique small molecule inhibitors, Bioorg. Med. Chem., 19 (2011) 4626-4634.
[19] S. Haider, C.G. Joseph, S. Neidle, C.A. Fierke, M.J. Fuchter, On the function of the internal cavity of histone deacetylase protein 8: R37 is a crucial residue for catalysis, Bioorg. Med. Chem. Lett., 21 (2011) 2129-2132.
[20] T. Castanheiro, J. Suffert, M. Donnard, M. Gulea, Recent advances in the chemistry of organic thiocyanates, Chemical Society Reviews, 45 (2016) 494-505.

- PD 404,182 is a isoenzyme selective HDAC8 inhibitor
- PD 404,182 reacts chemically with thiols yielding a thiophenol
- The mechanism-based inhibition of HDAC8 involves transient formation of a mixed disulfide
- PD 404,182 eventually modifies Cys153 yielding the corresponding isothiocyanate

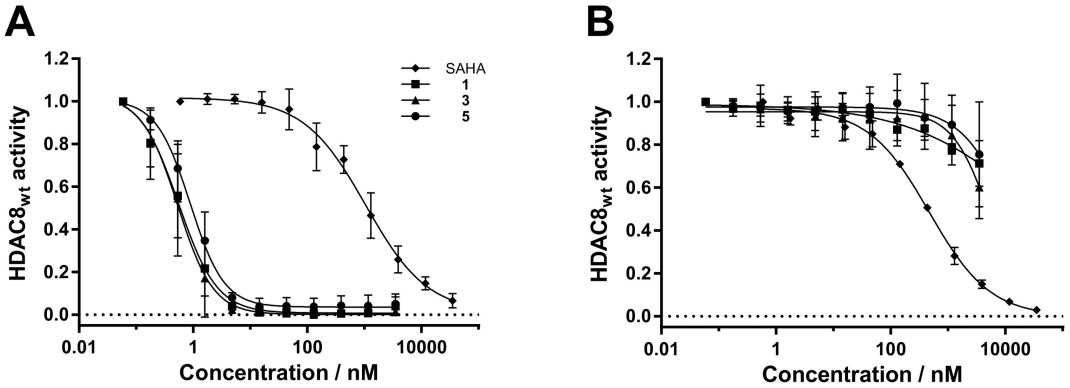
A
B
SAHA
1
3
5
HDAC8wt activity
Concentration / nM
0.0
0.2
0.4
0.6
0.8
1.0
1.2
0.01
1
100
10000

Figure 1

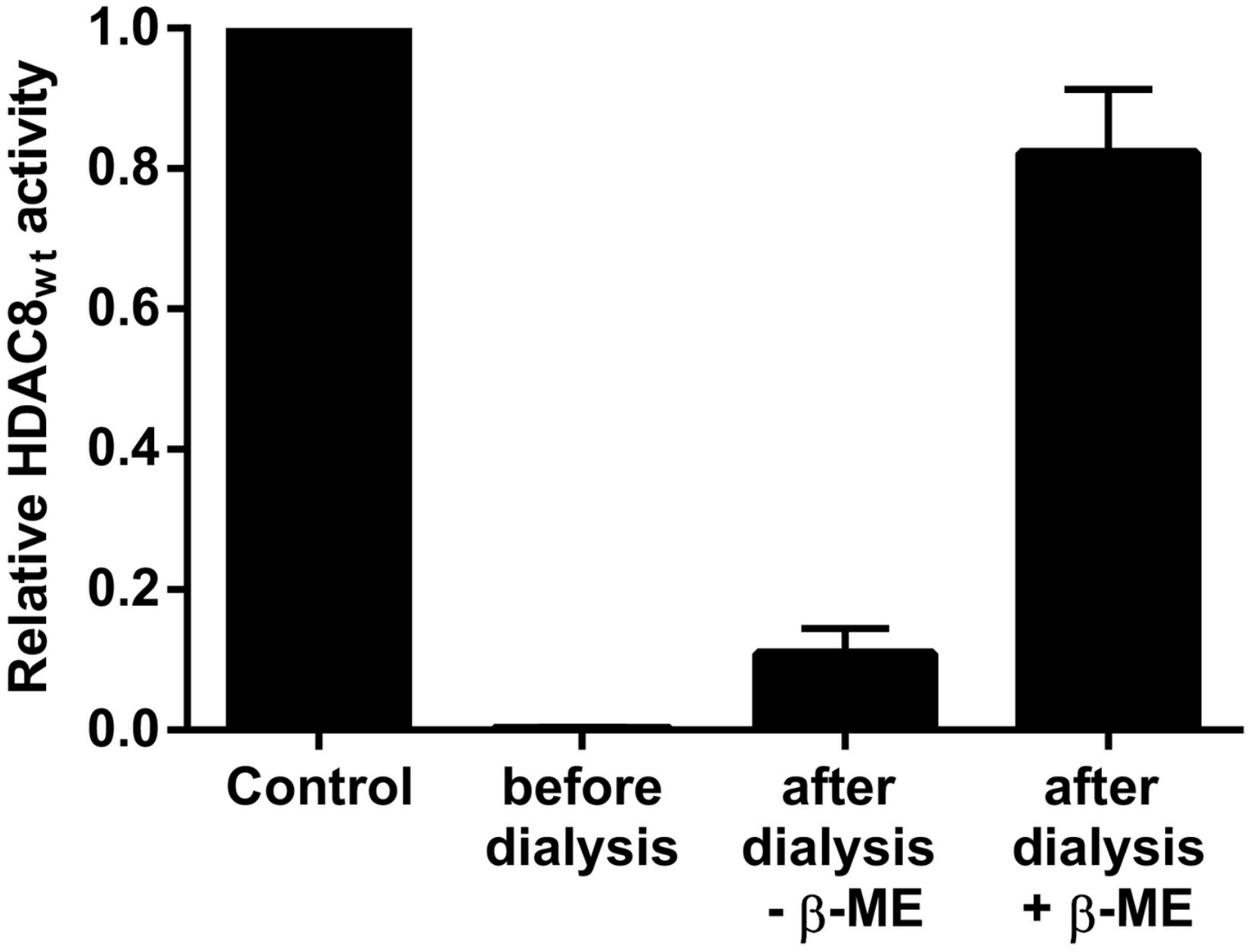
Relative HDAC8wt activity
1.0
0.8
0.6
0.4
0.2
0.0
Control
before dialysis
after dialysis - β-ME
after dialysis + β-ME

Figure 2

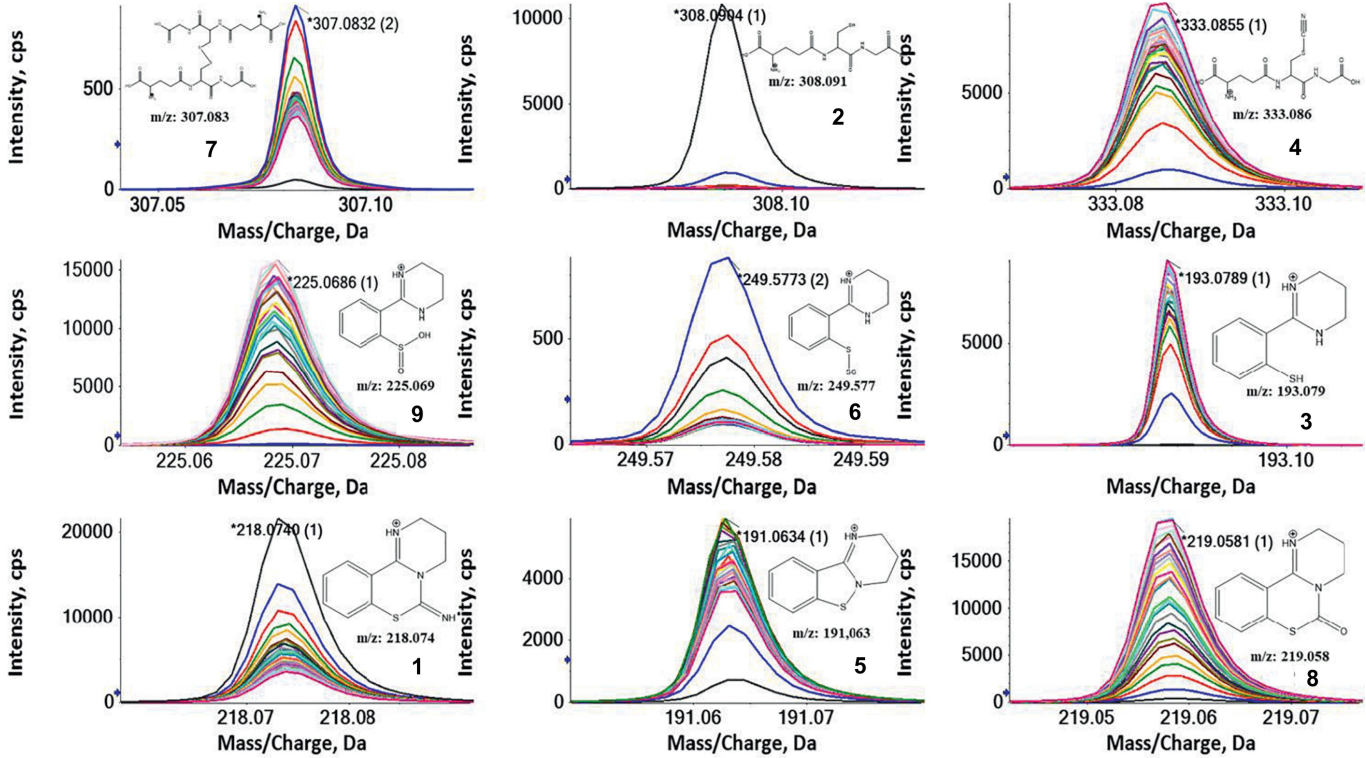
Intensity, cps
*307.0832 (2)
m/z: 307.083
7
307.05
307.10
Mass/Charge, Da
*308.0984 (1)
m/z: 308.091
2
308.10
*333.0855 (1)
m/z: 333.086
4
333.08
333.10
*225.0686 (1)
m/z: 225.069
9
225.06
225.07
225.08
*249.5773 (2)
m/z: 249.577
6
249.57
249.58
249.59
*193.0789 (1)
m/z: 193.079
3
193.10
*218.0740 (1)
m/z: 218.074
1
218.07
218.08
*191.0634 (1)
m/z: 191,063
5
191.06
191.07
*219.0581 (1)
m/z: 219.058
8
219.05
219.06
219.07
t [min] 0 35 70 105 140 175 210 245 280 315 350 385 420
455 490 525 560 595 630 665 700 735 770 805 840 875 910

Figure 3

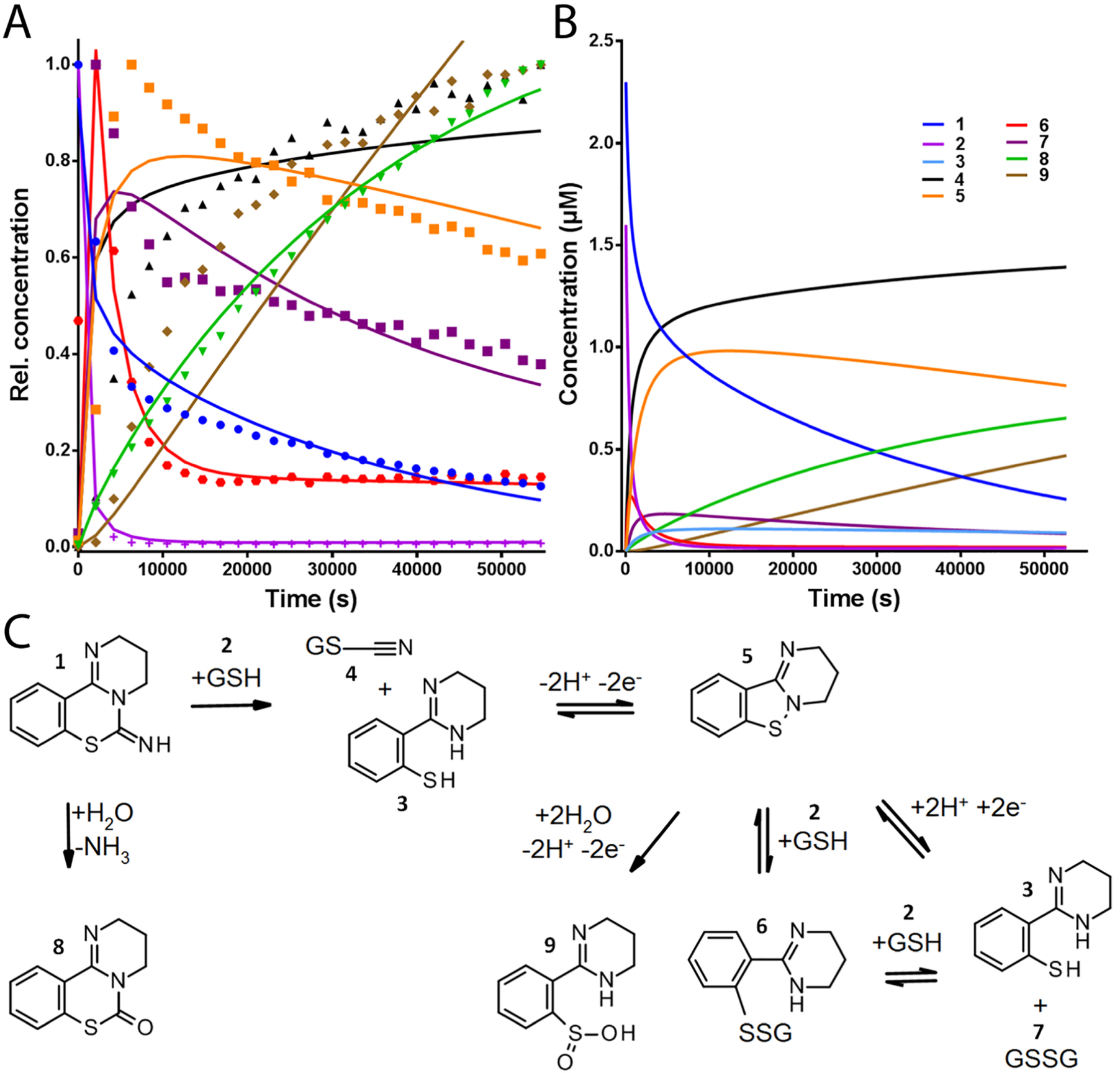
A
Rel. concentration
Time (s)
B
Concentration (μM)
Time (s)
1
2
3
4
5
6
7
8
9
C
+GSH
GS—≡N
4
3
-2H+ -2e-
5
+H2O
-NH3
8
+2H2O
-2H+ -2e-
9
2
+GSH
+2H+ +2e-
6
SSG
2
+GSH
3
+
7
GSSG

Figure 4

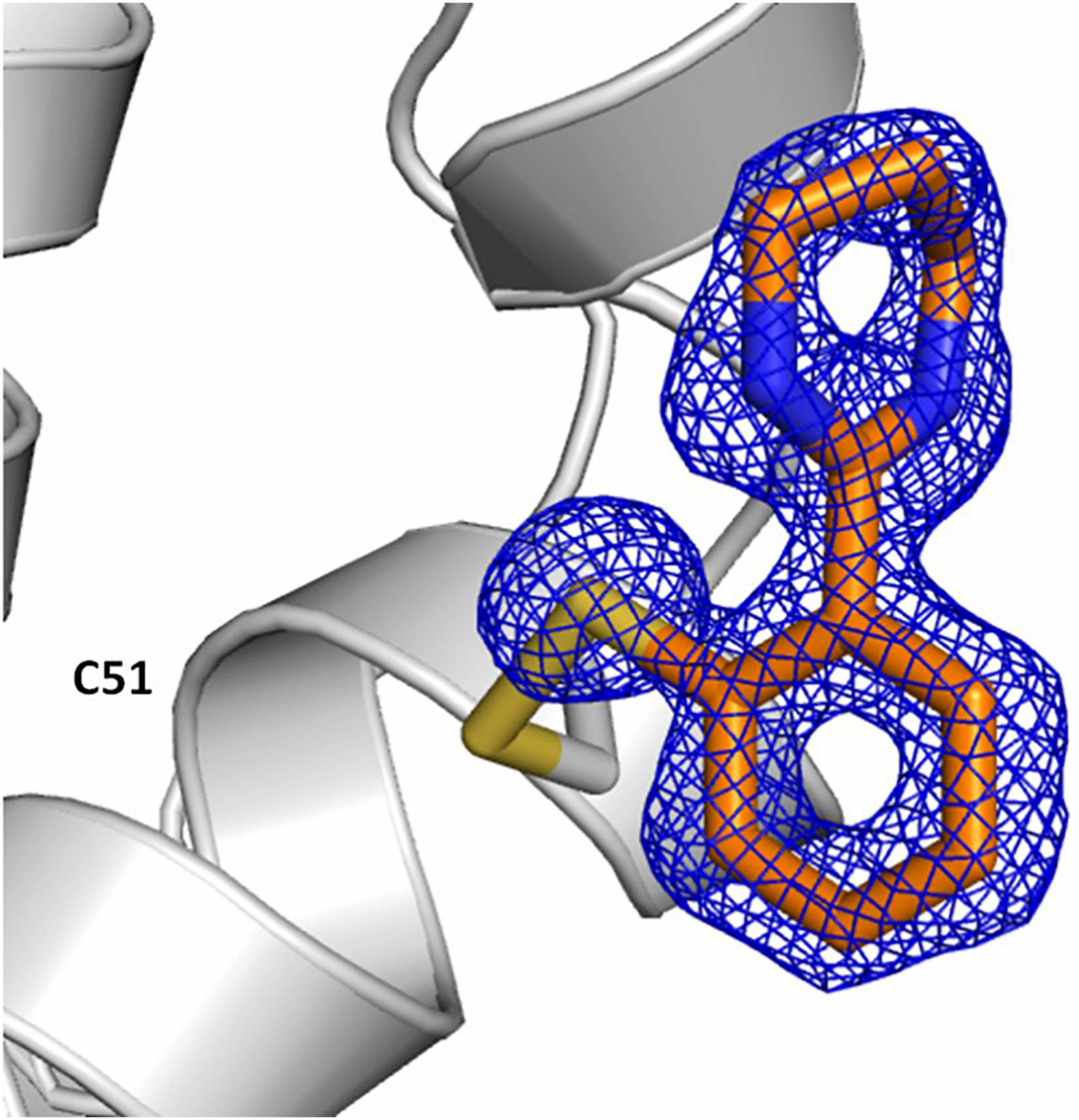

Figure 5

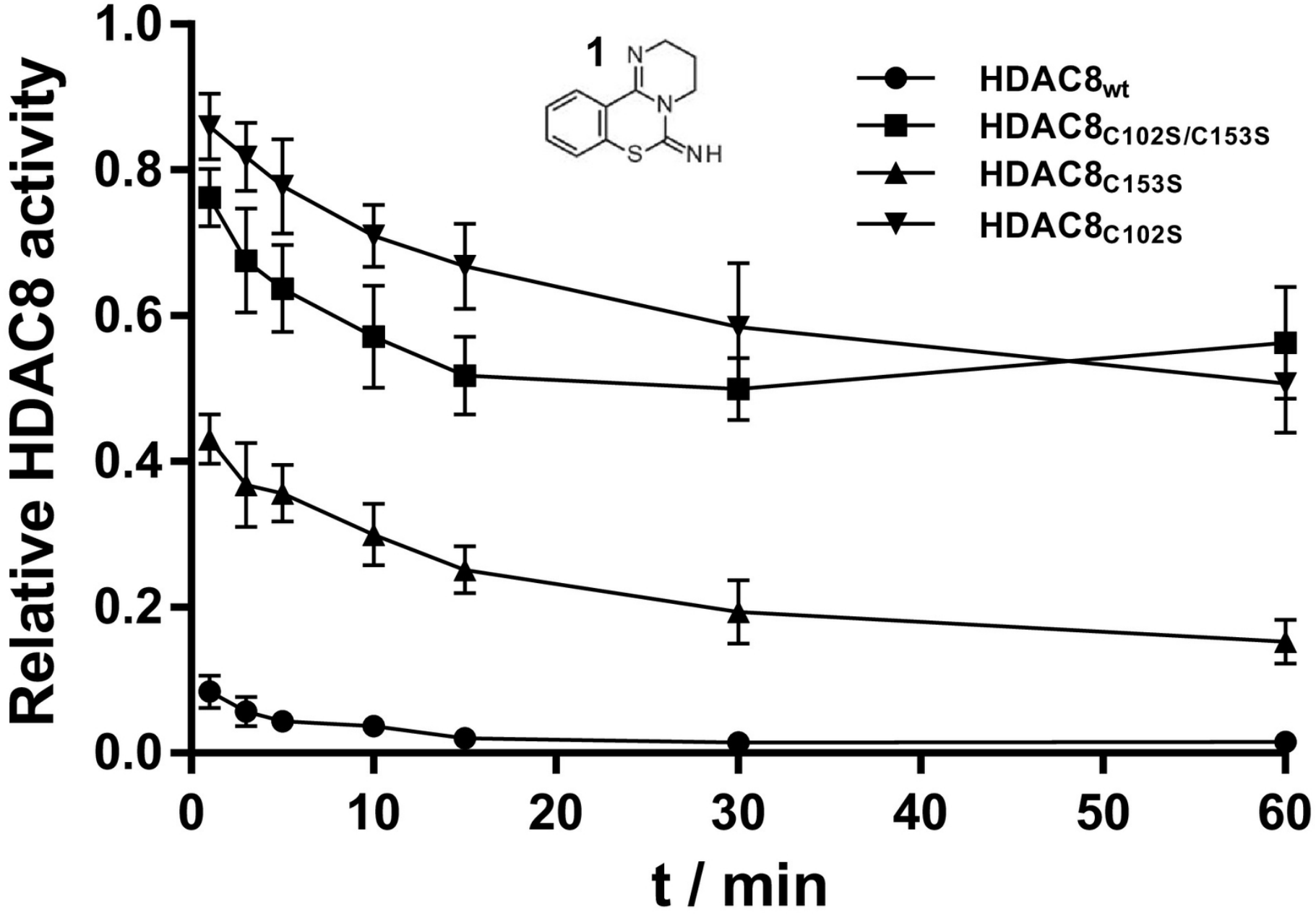
1
N
N
S
NH
HDAC8wt
HDAC8C102S/C153S
HDAC8C153S
HDAC8C102S
Relative HDAC8 activity
1.0
0.8
0.6
0.4
0.2
0.0
0
10
20
30
40
50
60
t / min

Figure 6

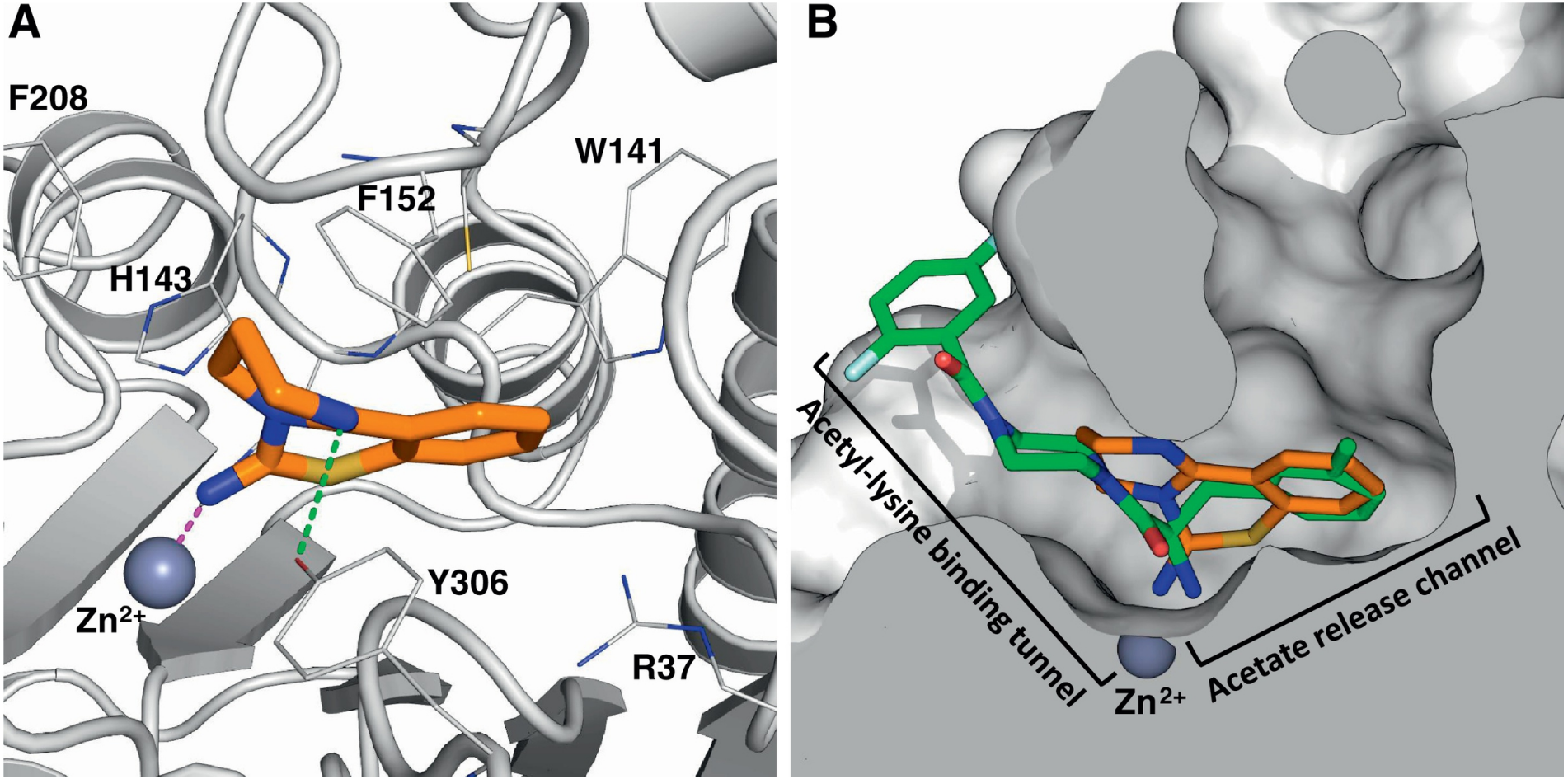
A
F208
W141
F152
H143
Y306
Zn2+
R37
B
Acetyl-lysine binding tunnel
Zn2+
Acetate release channel

Figure 7

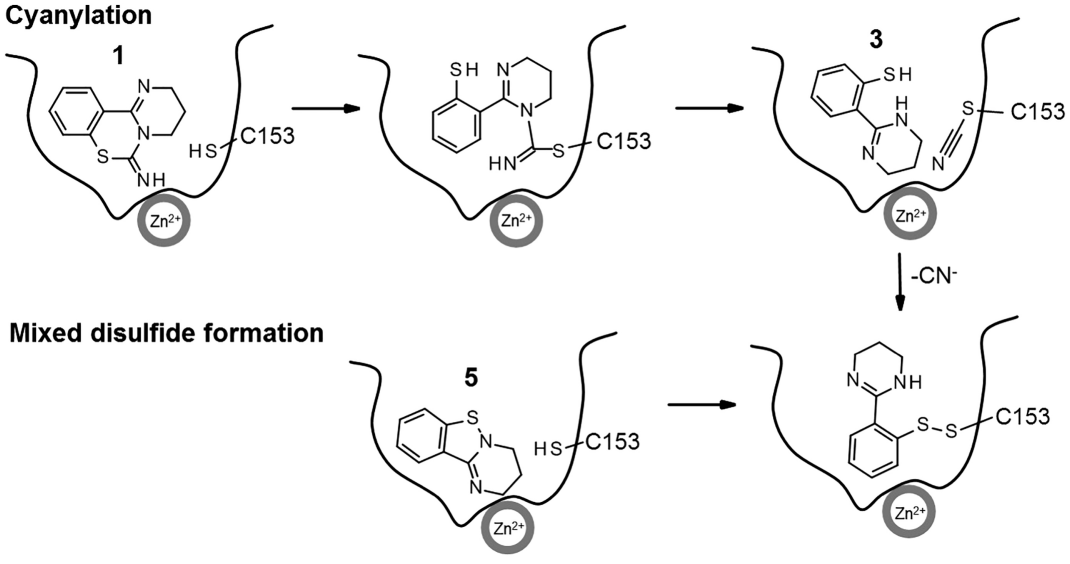
Cyanylation
1
HS C153
Zn2+
SH
HN
S C153
Zn2+
3
SH
NH
N
S C153
N
Zn2+
-CN-
Mixed disulfide formation
5
S
N
HS C153
N
Zn2+
N NH
S S C153
Zn2+

Figure 8